Available online at www.sciencedirect.com
SCIENCE DIRECT®
NeuroImage
ACADEMIC PRESS
NeuroImage 20 (2003) 393–403
www.elsevier.com/locate/ynimg

Research Article

A voxel-based morphometric study of nondemented adults with Down Syndrome

Nathan S. White,[a] Michael T. Alkire,[a] and Richard J. Haier[b,*]

[a] *Department of Anesthesiology, University of California at Irvine, Irvine, CA 92697, USA*
[b] *Department of Pediatrics, University of California at Irvine, Irvine, CA 92697, USA*

Received 13 January 2003; revised 28 March 2003; accepted 29 April 2003

Abstract

Previous structural brain imaging studies of Down Syndrome (DS) have offered important insights into the underlying morphometric aberrations associated with the condition. These previous studies have relied almost exclusively on classic region-of-interest (ROI)-based morphometry, a method in which a finite number of anatomical structures must be defined and delineated *a priori*. Here we use the fully automated voxel-based morphometry (VBM) approach on 19 nondemented individuals with DS and 11 age-matched controls in order to provide a full-brain assessment of DS morphology. Foci of statistically significant (P 0.05, corrected for multiple comparisons) reductions in gray matter (GM) tissue were observed in the cerebellum, cingulate gyrus, left medial frontal lobe, right middle/superior temporal gyrus, and the left CA2/CA3 region of the hippocampus. Significant decreases in white matter (WM) tissue were noted throughout the inferior brainstem. Foci of statistically significant (P 0.05, corrected for multiple comparisons) increases in GM tissue were observed in a superior/caudal portion of the brainstem and left parahippocampal gyrus. Significant increases in WM tissue were noted bilaterally in the parahippocampal gyrus. We also noted significant increases in cerebral spinal fluid in regions suggesting enlarged lateral ventricles in the DS group. While these results are generally consistent with prior ROI-based imaging studies of nondemented DS individuals, the present findings provide additional understanding of the three-dimensional topography of DS morphology throughout the brain. The consistency of these findings with prior imaging reports demonstrates the utility of the VBM technique for investigating the neuroanatomy of DS.

Introduction

Down Syndrome (DS), or trisomy 21, is the leading genetic cause of mental retardation in young adults (Nadel, 1999). Autopsy reports of DS individuals describe numerous neuropathologic observations, including reduced total brain volume, ventriculomegaly, and hypoplasia of the cerebellum, frontal lobe, temporal lobe, and brainstem (Zellweger, 1977; Kemper, 1991). Many of these studies have also reported hallmark pathologies of Alzheimer's disease (AD); a finding which is consistent with the high rate of occurrence of dementia in DS individuals over the age of 40 (Wisniewski et al., 1985). Recent structural imaging studies of DS, using CT and MRI technologies, show morphological abnormalities that parallel postmortem reports of DS neuropathology (Schapiro et al., 1989; Pearlson et al., 1990; Weis et al., 1991; Aylward et al., 1997a; Pinter et al., 2001b). In addition, these imaging studies have provided further insight into the potential cognitive repercussions of some of these morphometric aberrations (Raz et al., 1995; Aylward et al., 1999; Ikeda and Arai, 2002; Krasuski et al., 2002).

To date nearly all structural brain imaging studies of DS have relied exclusively on classic region-of-interest (ROI)-based volumetry. This method involves outlining individual structures across a series of contiguous brain slices and comparing the final cumulative volume of these structures across study cohorts. While advantageous in several respects, including increased sensitivity to volume changes in certain brain regions (Good et al., 2002; Tisserand et al., 2002), ROI volumetry has some limitations. In particular, it has been suggested that the interrater variability in identi-

* Corresponding author. Med Sci I, B140, University of California, Irvine, Irvine, CA 92697. Fax. 1-949-854-1989.
E-mail address: rjhaier@uci.edu (R.J. Haier).

1053-8119/03/$ – see front matter © 2003 Elsevier Inc. All rights reserved.
doi:10.1016/S1053-8119(03)00273-8

fying the boundaries of structures with complex surface geometries may lead to poor reproducibility (Hasboun et al., 1996; Pruessner et al., 2000; Chan et al., 2001). The technique also inherently introduces spatial biases, as inferences regarding morphometric differences are confined only to those brain regions encompassing the defined ROIs and tissues outside these regions are disregarded. Furthermore, because manually outlining individual structures is time-consuming and labor-intensive, many ROI studies only report findings on a small number of anatomical regions. As a result of these limitations, a full-brain comprehensive assessment of the structural neuroanatomy characteristic of living individuals with DS remains lacking in the literature.

Since its inception (Wright et al., 1995), voxel-based morphometry (VBM) has become an increasingly popular fully automated tool for providing an unbiased assessment of neuroanatomical differences throughout brain. The method is premised on making regionally specific (voxel-wise) inferences on the local relative concentrations (or absolute amounts after volumetric adjustments) of different tissue types after spatial normalization and segmentation of the underlying anatomical images (Ashburner and Friston, 2000). The results of the procedure are presented in standard stereotactic space which facilitates direct comparisons across studies. VBM has been extensively cross-validated with both ROI and functional analyses (Richardson et al., 1997; May et al., 1999; Good et al., 2002; Tisserand et al., 2002) and recently with particular reference to characterizing the neuroanatomic differences underlying different types of dementia (Good et al., 2002).

Here we performed VBM on nondemented individuals with DS. The goal of this study was to provide an objective, comprehensive assessment of the neuroanatomic abnormalities underlying DS in patients, prior to any onset of clinical signs of dementia.

Materials and methods

Subjects

The study group consisted of 19 (11 males, 8 females) individuals with DS (age range, 34–52; mean, 41.9; SD, 6.0; WAIS-III FSIQ range, 47–72; mean, 55.3; SD, 7.2) who showed absence of dementia as determined by the Dementia Scale for Down Syndrome (Deb and Braganza, 1999; Huxley et al., 2000) and the Dementia Questionnaire for Mentally Retarded Persons (Evenhuis, 1996) and 11 (5 males, 6 females) healthy age- and sex-matched controls (age range, 37–56; mean, 45.6; SD, 6.1; WAIS FSIQ range, 90–134; mean, 110.5; SD, 15.0). These subjects were recruited as part of a larger longitudinal study of dementia in Down Syndrome and Alzheimer's disease. All subjects gave informed consent in accordance with the University Institutional Review Board.

Image acquisition

T1-weighted, volumetric SPGR MRI scans (FOV, 24 cm; flip angle, 40°; TR, 24; TE, 5) were acquired on each subject using a 1.5-T clinical Phillips Eclipse scanner (Philips Medical Systems, N.A., Bothell, WA). The images consisted of 120 contiguous 1.2-mm-thick axial slices, each with an in-plane image matrix of 256 256 image elements. None of the DS subjects required sedation during the image acquisition as they all were high functioning and could follow directions. All images were visually inspected to ensure image quality.

Voxel-based morphometry

Voxel-based morphometry was performed following the methods detailed in Good et al. (2001). Only the portion of the preprocessing procedure pertinent to the present study is discussed below. Readers with additional inquires into the preprocessing methods are referred to Good et al. (2001) and Ashburner et al. (2000). All of the image processing procedures were performed using statistical parametric mapping software (SPM99, http//www.fil.ion.ucl.ac.uk/spm) implemented in Matlab 5.3 (MathWorks, Inc., Natick, MA).

Customized templates

The initial step of the VBM procedure was to create study-specific gray matter (GM), white matter (WM), and cerebral spinal fluid (CSF) templates. The impetus for developing these templates was to take into account the inherent variability in DS neuroanatomy from that of normal healthy subjects and to ensure that there would be no systematic errors introduced during the second-pass normalization/segmentation procedure (see below). The study-specific templates were created using the following approach: First, every image from the entire study (19 DS, 11 DS-controls) was spatially normalized to the default SPM99 T1-MRI template image that conforms to the stereotactic space defined by the atlas of Talairach and Tornoux (1988) and is based on 305 healthy subjects recruited from the Montreal Neurological Institute (MNI). The spatial normalization routine included both a 12-parameter linear affine transformation and a nonlinear transformation using a small set (1 1 1) of smoothed spatial basis functions (Ashburner and Friston, 1999). A small basis set was used to limit the deformations applied to the original images. The spatially normalized images were then segmented into GM, WM, and CSF partitions using a modified mixture model cluster analysis procedure with a correction for intensity non-uniformity and using *a priori* knowledge of the likelihood that a given voxel belongs to a certain tissue class (Ashburner and Friston, 1997). The resultant segmented images were then cleaned using a fully automated brain extraction procedure to remove scalp tissue, skull, and dural venous sinus voxels (Good et al., 2001) and individually

smoothed with an 8-mm full-width half-maximum (FWHM) isotropic Gaussian kernel. Study-specific GM, WM, and CSF templates were constructed by averaging all the respective GM, WM, and CSF smoothed images from all 30 subjects. The template images were written with a final isotropic resolution of 1.5 mm^3.

Normalization/segmentation

To facilitate the best possible partitioning of the respective tissue types, the study-specific GM, WM, and CSF templates were used as prior probability maps during a second-pass normalization/segmentation of the anatomical images. This time, however, the anatomical images, prior to segmentation, were spatially normalized using an optimal set of normalization parameters determined using the following approach: First, the raw anatomical images were segmented in native space resulting in a GM_{nat}, WM_{nat}, and CSF_{nat} image for each subject. Next, the images were cleaned using the brain extraction technique described previously. The cleaned GM_{nat}, WM_{nat}, and CSF_{nat} images were then spatially normalized (using a 12-parameter linear affine transformation and a nonlinear transformation using 7 8 7 nonlinear basis functions) to their respective study-specific template, yielding three sets of optimal normalization parameters for each subject. Then, depending upon the type of VBM analysis, one of the three sets of parameters was applied to the original anatomical image in native space. For the GM VBM analysis, the normalization parameters determined from the cleaned GM_{nat} images were used, for the WM VBM analysis, the normalization parameters determined from the cleaned WM_{nat} images were used, etc. The optimally normalized anatomical images were then segmented using the study-specific templates as prior probability maps. Nonbrain voxels were then removed from the final segmented GM, WM, and CSF partitions using the same brain extraction approach as mentioned above.

Modulation and smoothing

To preserve the amount of tissue in any given anatomical region after spatial normalization, the optimal GM, WM, and CSF partitions were multiplied by the Jacobian determinants of their respective spatial transformation matrix. The impetus for performing this modulation step was so that the final VBM statistics will reflect local deviations in the absolute amount (volume) of tissue in different regions of the brain (Ashburner and Friston, 2000). The modulated GM, WM, and CSF partitions were then smoothed with a 12-mm FWHM isotropic Gaussian kernel to account for slight misalignments of homologous anatomical structures and to ensure statistical validity under parametric assumptions. Additionally, to examine if expected *a priori* decreases of hippocampal gray matter could be found, in one analysis of gray matter tissue generated post-hoc, a 6-mm smoothing kernel was used.

Statistical analysis

Global effects

Total intracranial volumes (TIVs) were estimated by integrating the voxel values across the modulated (unsmoothed) GM, WM, and CSF partitions. Group differences in TIV as well as group differences in total GM, WM, and CSF volumes (after adjusting for TIV) were assessed using standard unpaired *t* tests.

Regionally specific effects

Regionally specific differences in GM, WM, and CSF volume were assessed within the context of the General Linear Model and Gaussian Random Field theory as implemented in SPM99 (Friston et al., 1995; Worsley et al., 1995). Statistical inferences were made at each voxel using an analysis of covariance (ANCOVA), with TIV, age, and sex treated as nuisance covariates. An absolute threshold was used to exclude voxels from the statistical comparison with intensities less than 0.05. Effects of interest were sought using linear contrasts of the parameter estimates and are presented as statistical parametric maps of the *t* statistic (SPM{*t*}s). As the primary objective of this report is to provide a broad perspective on the morphometric aberrations underlying DS, a threshold of P 0.001, uncorrected for multiple comparisons, was used in generating the figures and tables. However, only clusters surviving the correction for multiple comparisons at P 0.05 are addressed in the Discussion. These statistical criteria were relaxed in the case of the post hoc reanalysis of the GM images smoothed with a 6-mm kernel. Because there was a strong *a priori* prediction for GM decreases in the hippocampus, we used a small volume correction for this region instead of the whole brain correction. More specifically, the hippocampal effects were corrected using a 40 40 40 mm^3 sphere (9929 voxels), which approximates the volume of the hippocampal region and has been used in previous studies of hippocampal morphology using VBM (Maguire et al., 2000; Kubicki et al., 2002). The figure for this post hoc reanalysis is presented at the whole brain P 0.05 uncorrected level for illustration purposes. Regional effects were localized according to the atlas of Talairach and Tournoux (1988) after adjustment for differences between Talairach and MNI coordinates using a linear transformation developed by M. Brett (http://www.mrc-cbu.cam.ac.uk/Imaging/mnispace.html).

Results

Global effects

Consistent with previous studies on DS neuroanatomy (Schapiro et al., 1989; Haier et al., 1995; Pearlson et al., 1998; Aylward et al., 1999; Pinter et al., 2001a, 2001b), we observed a significant decrease (P 0.007) in DS TIV when compared to their control group (DS: mean, 1270

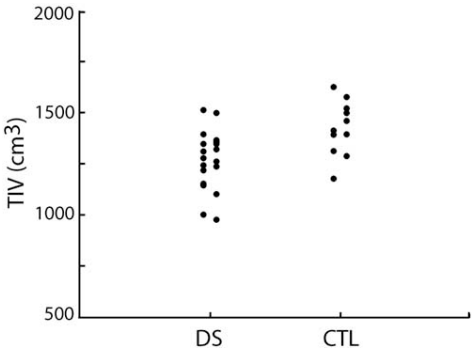

Fig. 1. Scatterplot of total intracranial volume (TIV) for the DS and control (CTL) groups.

cm^3, SD, 140 cm^3; DS-control: mean, 1430 cm^3, SD, 130 cm^3); see Fig. 1. However, we did not find a difference in the adjusted total GM (P 0.35), WM (P 0.65), or CSF (P 0.15) volumes between our study groups.

Regionally specific effects

Illustrated in Fig. 2 is the SPM99 design matrix. This matrix is a graphical representation of the statistical ANCOVA performed on the smoothed segmented images. Each column in the design matrix corresponds to a modeled effect and each row corresponds to a subject's scan. The last three columns of the design matrix model the confounding effects of TIV, age, and sex on the data; see Fig. 2 legend for more details about the design matrix. The regionally specific effects are listed in Tables 1–3. Those regions whose coordinates and Z statistics are in bold lettering are the global maxima of the tabled clusters, while those regions not in bold lettering are the local maxima. In Table 1, SVC is an acronym for "small volume correction."

Gray matter

Regional changes in GM volume, having factored out the effects of TIV, age, and sex, are listed in Table 1 and shown in Fig. 3. The DS group evidenced reduced GM volume predominately in the cerebellum, left medial frontal lobe, right superior/middle temporal lobe, and throughout a large portion of the cingulate gyrus. Significant increases in GM volume were observed in a superior/caudal portion of the brainstem, which extended superiorly and laterally into the left parahippocampal gyrus. The post hoc GM reanalysis revealed significant decreases in the CA2/CA3 region of the left hippocampal gyrus (Fig. 6). While this effect appears to be bilateral, only the left hippocampal finding survives the small volume correction (P 0.05, SVC).

White matter

Regional changes in WM volume, having factored out the effects of TIV, age, and sex, are listed in Table 2, and shown in Fig. 4. The DS group showed less WM volume throughout the brainstem and more WM volume in both the left and right parahippocampal gyrus.

Cerebral spinal fluid

Regional changes in CSF volume, having factored out the effects of TIV, age, and sex are listed in Table 3, and shown in Fig. 5. The DS group evidenced higher levels of CSF in the lateral ventricles and lower levels surrounding an inferior portion of the orbital frontal cortex.

Discussion

Primary findings

Here we present a number of gross morphometric abnormalities in DS neuroanatomy by characterizing regional volumetric aberrations in GM, WM, and CSF using VBM. In descending order of statistical significance and after controlling for the effects of TIV, age, and sex, we found extensive GM reductions in the cerebellum, right medial/superior temporal lobe, left medial frontal lobe, as well as a large area encompassing both the anterior and middle portions of the cingulate gyrus. WM reductions were observed principally in brainstem with an effect that extended inferior–superiorly from the basal pons up to the level of the substantia nigra and owning a statistical maximum in the left inferior cerebellar peduncle. The pattern of regional tissue loss tended to be bilateral, although only those regions that remained after a full-brain statistical correction for multiple comparisons are mentioned above. For consistency, we also tested for increases in region tissue volumes that revealed significant GM increases in a superior/caudal region of the brainstem, an effect that extended superiorly and laterally into the left parahippocampal gyrus, and robust WM increases in both the left and right parahippocampal

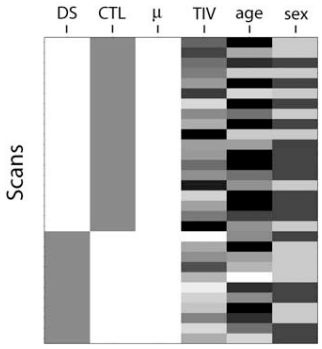

Fig. 2. SPM99 design matrix for the VBM analysis. The first two columns model the main effect of condition (group effect), and the last three columns model the confounding effects of TIV, age, and sex, respectively. Each row corresponds to a subject's scan. The third column models the mean of the data across subjects. A linear contrast across the first two columns tests for structural differences between the DS and control groups.

Table 1
Locations of regional aberrations in gray matter volume

k	Region	Coordinates (mm)			*Z*
		x	*y*	*z*	
Down Syndrome controls					
10475*	L. cerebellum	**3**	**71**	**18**	**5.02****
	R. cerebellum	18	66	27	4.51
	R. cerebellum	26	59	30	4.42
5123*	R. sup. temporal gyrus	**45**	**20**	**0**	**4.68****
	R. mid. temporal gyrus	48	33	5	4.64**
	R. sup. temporal gyrus	74	20	8	4.14
3055*	L. med. frontal gyrus/ant. cingulate gyrus	**9**	**59**	**11**	**4.52**
	L. med. frontal gyrus/ant. cingulate gyrus	23	72	8	4.51
	R. med. frontal gyrus/ant. cingulate gyrus	8	54	11	3.79
650	R. thalamus	**8**	**24**	**20**	**4.31**
4162*	R. med. frontal gyrus/cingulate gyrus	**11**	**9**	**56**	**4.30**
	R. med. frontal gyrus/cingulate gyrus	14	17	47	4.18
	L. med. frontal gyrus/cingulate gyrus	8	15	45	4.06
130	L. cuneus	**18**	**84**	**21**	**3.85**
1041	L. mid. frontal gyrus	**65**	**47**	**3**	**3.81**
	L. sup. temporal gyrus	71	48	14	3.72
	L. sup. temporal gyrus	71	30	6	3.52
31	R. mid. frontal gyrus	**32**	**33**	**5**	**3.46**
150	L. sup. temporal gyrus	**47**	**20**	**3**	**3.39**
63	L. precentral gyrus	**38**	**21**	**54**	**3.38**
94	R. hypothalamus	**6**	**0**	**6**	**3.38**
41	R. mid. frontal gyrus	**29**	**51**	**12**	**3.34**
63	L. mid. occipital gyrus	**47**	**69**	**8**	**3.29**
28	L. orbital/rectal gyrus	**2**	**45**	**26**	**3.25**
17	L. inf. temporal gyrus	**48**	**18**	**32**	**3.17**
19	L. inf. temporal gyrus	**53**	**6**	**41**	**3.16**
121	L. hippocampus***	**36**	**23**	**12**	**4.39**
553	R. hippocampus	38	20	15	3.49
Down Syndrome controls					
4985*	R. brainstem	**8**	**36**	**5**	**4.53**
	L. brainstem	15	48	8	4.16
33	R. caudate	**5**	**23**	**6**	**3.71**
886	R. orbital/rectal gyrus	**9**	**20**	**29**	**3.71**
	L. orbital/rectal gyrus	8	20	29	3.64
107	R. sup. parietal lobule	**9**	**68**	**62**	**3.56**
212	L. sup. parietal lobule	**6**	**66**	**62**	**3.47**
	L. sup. parietal lobule	15	69	60	3.35
59	R. inf. frontal gyrus	**23**	**20**	**11**	**3.30**
29	Undefined (nonbrain)	**12**	**12**	**50**	**3.26**
6	Occipital lobe	**33**	**59**	**15**	**3.24**

* P 0.05, corrected (cluster level).
** P 0.05, corrected (voxel level).
*** P 0.05, SVC, k cluster size (in voxels).

gyrus. Increases in regional CSF were also noted in areas suggesting significant dilations of the lateral ventricles in the DS group.

Using the analysis methods detailed above with a 12-mm smoothing kernel, we did not observe any reductions in hippocampal volumes in our DS cohort. This contrasts with a number of previous imaging studies based on the ROI method (Emerson et al., 1995; Pearlson et al., 1998; Aylward et al., 1999; Pinter et al., 2001a). Given that a decrease in hippocampal volume is noted fairly consistently throughout the DS literature, and a number of studies exist that cross-validated the VBM method with the ROI method in detecting hippocampal atrophy under various neuropathologic conditions (Good et al., 2002; Keller et al., 2002; Kubicki et al., 2002), we considered the possibility that the lack of hippocampal changes found here could have been a result of the large spatial smoothing kernel (12 mm) typically used with VBM analyses. To explore this idea we reanalyzed the GM data with a 6-mm smoothing kernel testing explicitly for decreases of hippocampal volume. The results of this reanalysis are shown in Fig. 6. For clarity, Fig. 6 only includes regional decreases in GM volume.

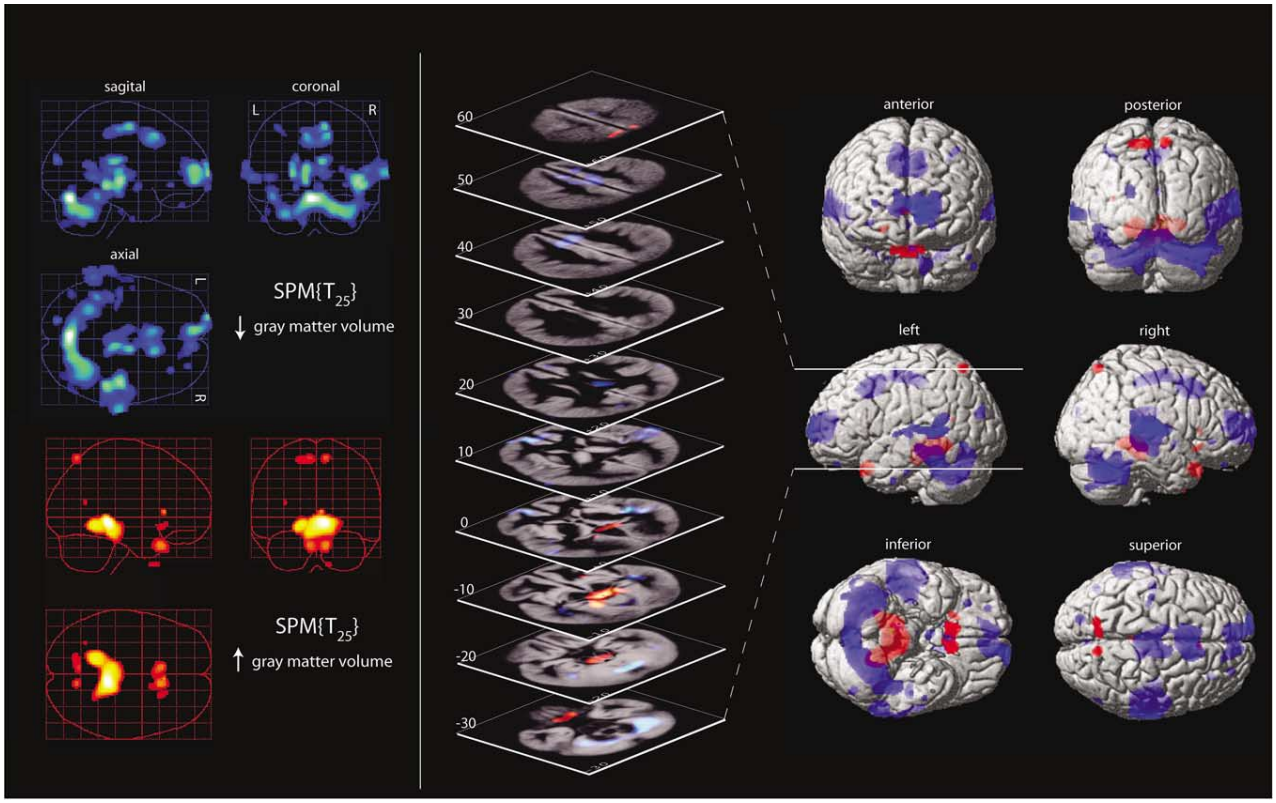

3

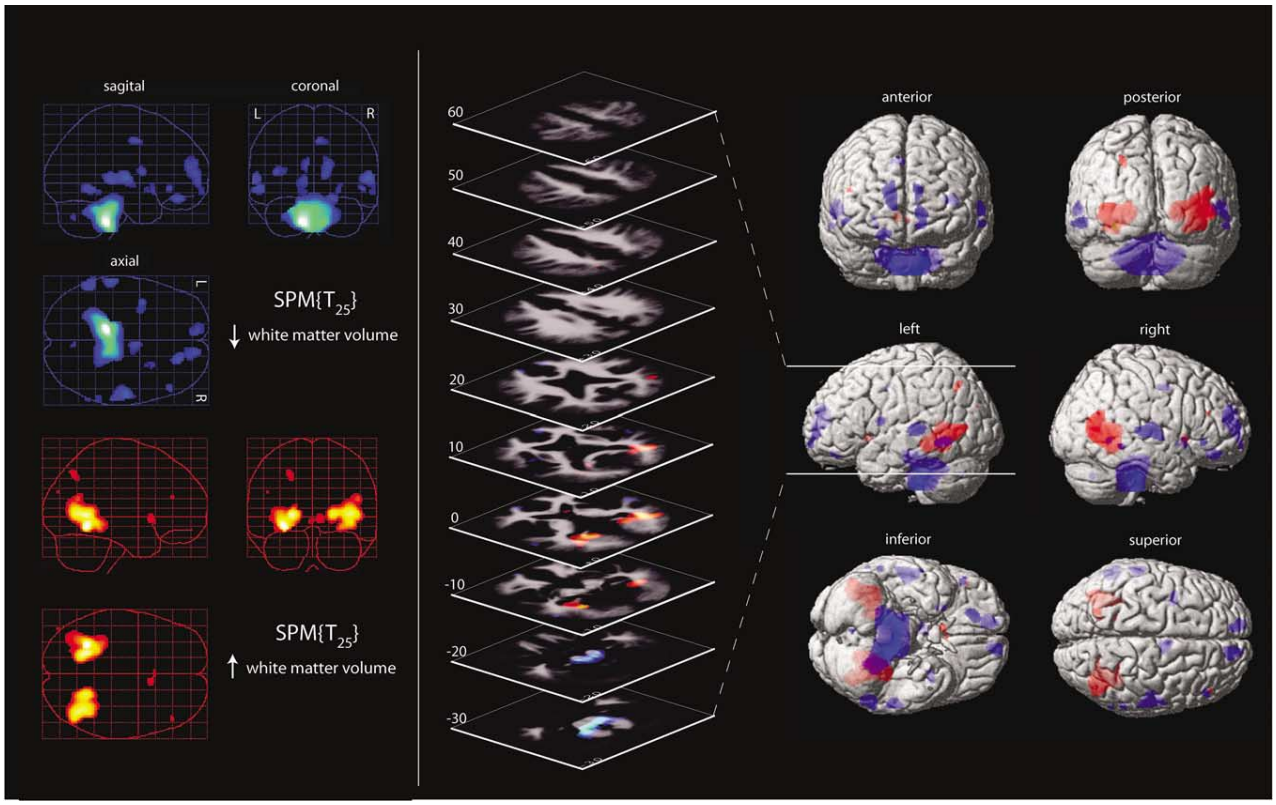

4

Fig. 3. Regionally specific changes in GM volume. Significant decreases and increases in DS regional gray matter volume are shown in blue and red, respectively. On the far lefthand side of the figure are the resultant GM statistical parametric maps (SPMs) shown as maximum intensity projections (MIPs) onto a standard"glass brain." The intensity of the projections illustrates the strength of the significance. Surface renderings (in six orthogonal views) of these SPMs are shown on the far righthand side of the figure. The renderings are displayed on a standard T1 anatomical image in Talariach space. In the middle of the figure are a series of 10-mm axial "cuts" though the brain with respective *z* coordinates. The approximate locations of these cuts are shown on one of the surface renderings. The underlying axial images are those of the study-specific gray matter template. The images are rotated 45° CW to aid visualization.

Fig. 4. Regionally specific changes in WM volume. Significant decreases and increases in DS regional white matter volume are shown in blue and red, respectively. The underlying axial images in the middle of the figure are those of the study-specific white matter template. Refer to Fig. 3 for a detailed explanation of the figure layout.

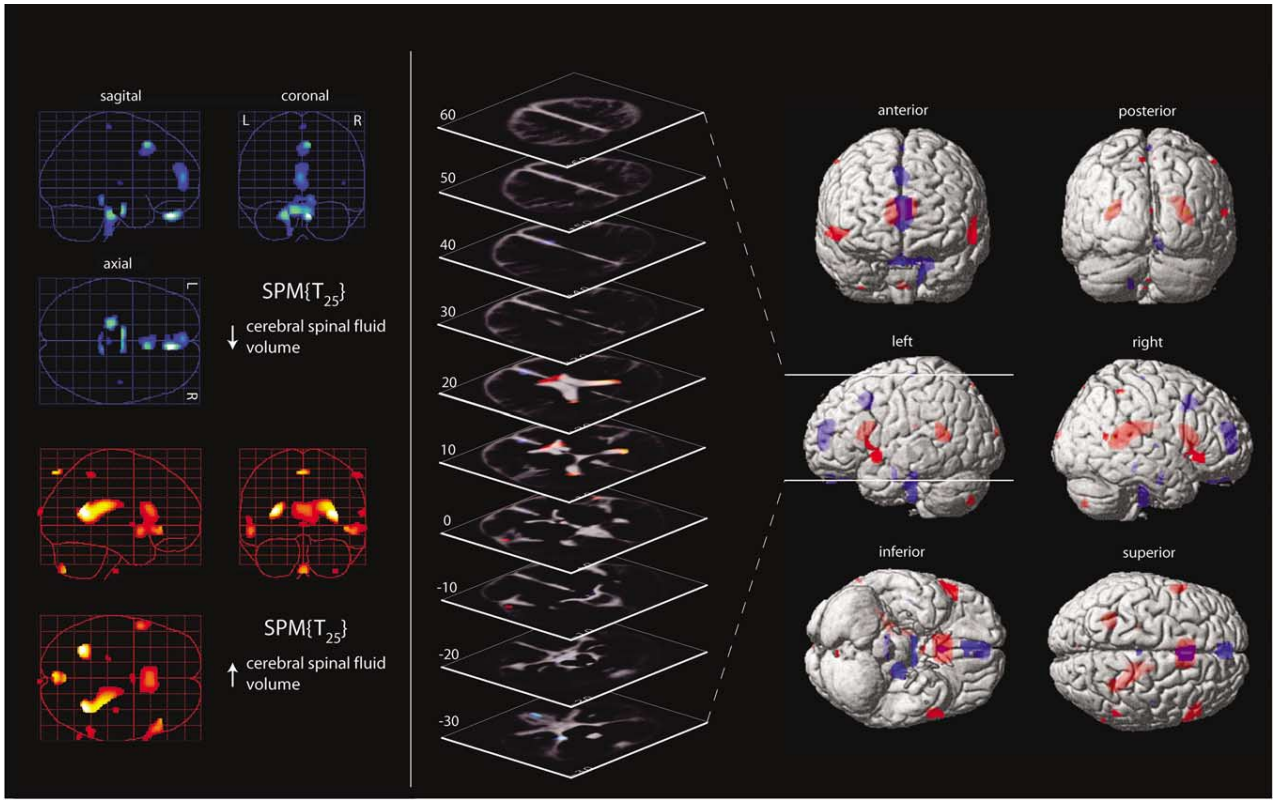

5

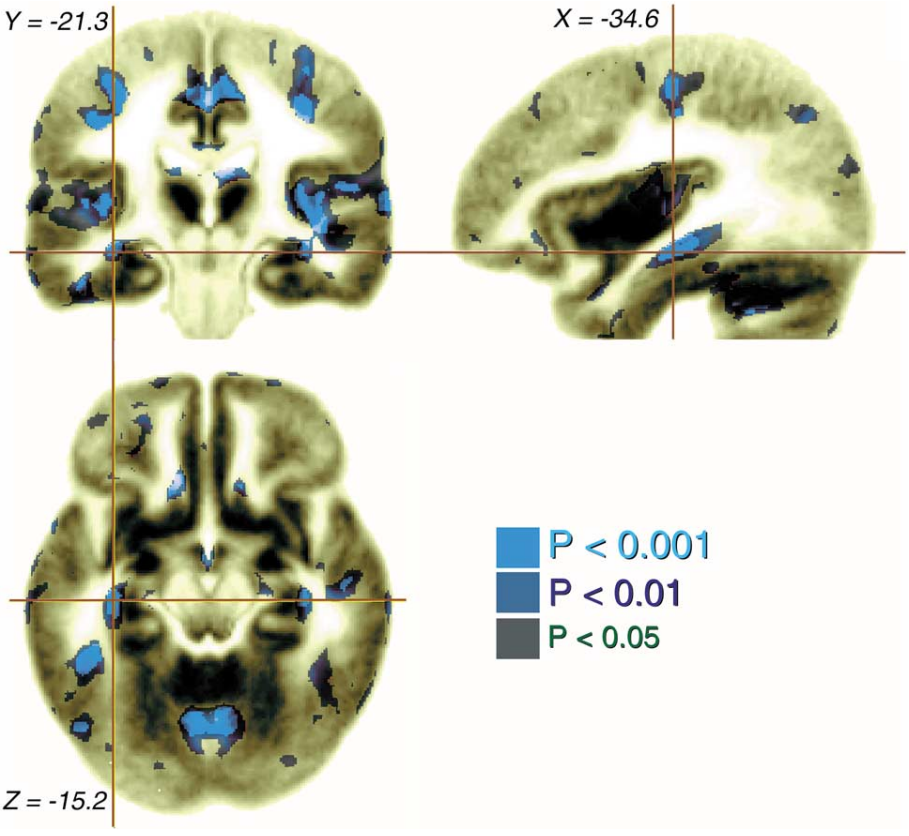

6

Fig. 5. Regionally specific changes in CSF volume. Significant decreases and increases in DS regional CSF volume are shown in blue and red, respectively. The underlying axial images in the middle of the figure are those of the study-specific CSF template. Refer to Fig. 3 for a detailed explanation of the figure layout.
Fig. 6. VBM analysis of GM volume decreases in DS using a 6-mm smoothing kernel. Results of decreased GM volume in DS relative to controls are shown superimposed on a T2 version of the GM study-specific template image. Given the strong *a priori* expectation for decreased GM volume in the hippocampal region, the results are shown at various *P* values ranging from *P* 0.05 to *P* 0.001, uncorrected. A clear effect is evident bilaterally in the hippocampus, which seems to center around the CA2 and CA3 regions.

Table 2
Locations of regional aberrations in white matter volume

k		Region	Coordinates (mm)			*Z*
			x	*y*	*z*	
Down Syndrome	controls					
8477*		L. brainstem	**11**	**35**	**41**	**5.92****
		R. brainstem	9	30	42	5.13**
543		R. sup. temporal gyrus	**57**	**14**	**6**	**4.26**
		R. sup. temporal gyrus	62	26	5	3.96
222		L. sup. temporal gyrus	**63**	**30**	**3**	**4.14**
184		R. sup frontal gyrus	**20**	**41**	**17**	**4.09**
260		L. inf. temporal gyrus	**57**	**53**	**6**	**3.96**
129		R. cingulate gyrus	**5**	**5**	**45**	**3.74**
132		L. insula	**39**	**3**	**12**	**3.62**
479		R. med. frontal gyrus	**11**	**59**	**9**	**3.62**
		R. sup. frontal gyrus	15	51	18	3.57
210		L. med. frontal gyrus	**9**	**60**	**2**	**3.56**
		L. sup. frontal gyrus	11	65	9	3.31
33		R. inf. frontal gyrus	**51**	**30**	**6**	**3.55**
113		L. med. frontal gyrus	**8**	**56**	**18**	**3.54**
11		R. inf. semi-lunar lobule	**5**	**69**	**35**	**3.42**
24		R. claustrum	**26**	**14**	**8**	**3.39**
27		R. mid. temporal gyrus	**62**	**44**	**9**	**3.33**
9		R. inf. temporal gyrus	**63**	**54**	**3**	**3.33**
4		R. putamen	**27**	**8**	**5**	**3.29**
1		R. putamen	**24**	**9**	**8**	**3.28**
Down Syndrome	controls					
3374*		L. parahippocampal gyrus	**30**	**54**	**9**	**4.93****
		L. lingual gyrus	21	56	2	4.69**
4311*		R. parahippocampal gyrus	**41**	**63**	**3**	**4.55****
		R. lingual gyrus	23	56	3	4.50**
		R. mid. temporal gyrus	47	63	18	3.69
53		R. caudate	**8**	**14**	**2**	**3.43**
66		L. sup. parietal lobule	**24**	**68**	**45**	**3.32**
8		R. mid. frontal gyrus	**47**	**36**	**20**	**3.25**
7		L. ant. cingulate gyrus	**2**	**17**	**5**	**3.15**
1		L. mid. temporal gyrus	**47**	**84**	**26**	**3.12**

* P 0.05, corrected (cluster level).
** P 0.05, corrected (voxel level); k cluster size (in voxels).

Using this smaller smoothing kernel, the expected decreases in hippocampal volumes become evident at a fairly robust significance level of P 0.001, uncorrected.

Our findings of reduced total brain volumes accompanied by disproportionately smaller cerebellar, brainstem, and frontal lobe volumes are consistent with a large body of both prior neuroimaging and postmortem evidence (Zellweger, 1977; Schapiro et al., 1989; Pearlson et al., 1990; Wisniewski, 1990; Kemper, 1991; Weis et al., 1991; Haier et al., 1995; Aylward et al., 1997a; Nadel, 1999; Pinter et al., 2001b). While often not a target in conventional imaging studies of DS, we observed robust decreases in GM volume throughout a large expanse of the anterior and middle portions of the cingulate gyrus, a finding that is consistent with the work of Raz and colleagues (1995). We also noted GM loss in a large portion of the right temporal lobe that covered an extent of the middle and superior temporal gyrus, posterior insula cortex, and the transverse temporal gyri. This is consistent with prior imaging studies (Kesslak et al., 1994; Raz et al., 1995) and postmortem evidence (Burger and Vogel, 1973; Becker et al., 1986; Takashima et al., 1989; Wisniewski, 1990). Regional increases in DS WM volume were found bilaterally in the parahippocampal gyri, a finding that also appears to be consistent with a few prior reports based on the ROI method (Kesslak et al., 1994; Emerson et al., 1995; Raz et al., 1995).

Many of the aforementioned regional results have been reported in prior ROI-based imaging studies of DS morphology, but these results appear somewhat inconsistent throughout the literature. For example, Aylward and colleagues (1997a) reported reduced putamen volumes in their group of DS individuals, whereas Raz and co-workers (1995) failed to find such a difference despite using subjects with similar cognitive and physical profiles. Contributing to inconsistencies of this nature could be a number of methodological factors associated with the ROI method, including (1) the interrater and intrarater variability in outlining anatomical structures, (2) the arbitrary selection criteria of the ROIs in any given study (i.e., not all studies outline the same anatomical structures and use the same boundary

Table 3
Locations of regional aberrations in cerebral spinal fluid volume

k		Region	Coordinates (mm)			*Z*
			x	*y*	*z*	
Down Syndrome	controls					
282		R. orbital gyrus	**8**	**41**	**30**	**4.65****
		L. orbital gyrus	5	38	29	3.18
354		L. pons	**18**	**24**	**29**	**4.26**
		L. brainstem	12	24	48	3.43
301		L. brainstem	**8**	**11**	**26**	**4.25**
		R. brainstem	5	11	26	3.93
432		R. med. frontal gyrus	**6**	**15**	**47**	**4.11**
852		L. med. frontal gyrus	**2**	**54**	**11**	**3.79**
81		R. brainstem	**9**	**33**	**12**	**3.77**
		L. brainstem	3	35	12	3.29
15		R. med. frontal gyrus	**2**	**26**	**66**	**3.21**
5		R. insula	**45**	**14**	**5**	**3.12**
Down Syndrome	controls					
321		L. lateral ventricle	**30**	**56**	**15**	**4.52****
1475*		R. lateral ventricle	**33**	**53**	**12**	**4.48****
		R. lateral ventricle	29	35	20	4.04
86		L. sup. parietal lobule	**2**	**84**	**57**	**3.98**
311		R. inf. frontal gyrus	**47**	**29**	**3**	**3.77**
		R. inf. frontal gyrus	54	26	6	3.67
89		R. cerebellum	**2**	**74**	**50**	**3.77**
1503		L. lateral ventricle	**2**	**17**	**18**	**3.64**
293		L. sup. temporal gyrus	**56**	**8**	**5**	**3.62**
		L. precentral gyrus	57	15	5	3.22
22		R. sup. temporal gyrus	**63**	**60**	**15**	**3.38**
52		R. inf. parietal lobule	**57**	**48**	**53**	**3.32**
13		Undefined (nonbrain)	**35**	**20**	**50**	**3.28**
10		L. cuneus	**3**	**101**	**15**	**3.26**
17		Third ventricle	**0**	**2**	**2**	**3.15**
7		L. lateral ventricle	**21**	**27**	**21**	**3.12**

* P 0.05, corrected (cluster level).
** P 0.05, corrected (voxel level), k cluster size (in voxels).

protocols), and (3) the differences in the way the independent measures (i.e., tissue volumes) are controlled for across studies. The advantage of VBM is that it provides an unbiased, full-brain assessment of regional morphology devoid of any *a priori* assumptions or subjective input, lending the first two points above irrelevant when making regional inferences. Although the results presented here do not provide a definitive answer into how the putamen may be structurally different in DS individuals, we did notice a reduction (P 0.001, uncorrected) in the volume of the right putamen, consistent with the work of Aylward and colleagues (1997b).

An additional advantage of the VBM method over the traditional ROI method is that in certain situations VBM may offer increased sensitivity to regional pathology over the conventional ROI method. This is because the traditional method of drawing regions of interest asserts a generalized homogenous distribution of pathology within these regions. If the pathology is regionally specific beyond the spatial scale of the circumscribed ROI, then the traditional method of "counting voxels" may be prone to false negatives. The VBM method is not limited in this respect and the foci of the statistical parametric maps may offer additional insight into such regional pathology. As demonstrated in Fig. 6, the foci of these statistical maps suggest that our DS cohort had hippocampal atrophy (or hypoplasia) that seemed to be most prominent in the CA2/CA3 subregions.

The VBM method, however, also has limitations. All voxel-based approaches, like VBM, require the data to be spatially normalized into a standardize space. Systematic registration errors of the resultant images may lead to spurious effects in the VBM comparisons. To account for this potential risk, and in order for the statistical inferences to be valid under parametric assumptions, the normalized images are often blurred with a substantial spatial smoothing kernel (Salmond et al., 2002). In this study, we demonstrate that in small structures like the hippocampus, this spatial smoothing requirement may subject the VBM method to false negatives as well. It was not until we reduced the size of the spatial smoothing kernel that we were able to clearly detect the decreases in hippocampal GM tissue that have been reported extensively throughout the DS literature.

AD neuropathology in DS

All DS individuals by the 4th decade show some degree of tangle and plaque neuropathology similar to that of AD (Wisniewski et al., 1985) which is due to the overexpression of the amyloid precursor protein gene location on chromosome 21 (Kang et al., 1987; Tanzi et al., 1988). Provided accurate in vivo measurements are made, DS cohorts may offer significant insight into both the prodromal phase and progression of AD neuropathology. In the current study we demonstrate numerous neuroanatomical abnormalities in DS individuals who are without any clinical signs of dementia. However, the etiology of these abnormalities can't be determined from these data. Even though the current findings overlap well with VBM reports of AD (Baron et al., 2001; Chan et al., 2001) it remains to be determined to what extent this DS morphology is a result of a generalized pathology due to the amyloid protein or a result of abnormal neurodevelopmental processes. This is especially important with regard to temporal lobe regions, which are some of the first structures affected in AD. We believe that this study is important because it helps establish the utility of the VBM methology for studying DS temporal lobe neuroanatomy and, consequently, provides a platform from which further comparative study can be made between AD and DS.

Conclusion

To our knowledge, this study provides the first full-brain objective account of the gross structural brain abnormalities inherent in living nondemented individuals with DS. The consistency of the present findings with evidence from prior imaging and postmortem reports provide support for the VBM technique in assessing neuroanatomic aberrations in DS individuals.

Acknowledgments

This research was funded by Grant RO1 HD37427 (Dr. Haier, PI) from NICHD. The authors thank Elizabeth Head for helpful comments on the manuscript.

References

Ashburner, J., Friston, K., 1997. Multimodal image coregistration and partitioning—a unified framework. Neuroimage 6 (3), 209–217.

Ashburner, J., Friston, K.J., 1999. Nonlinear spatial normalization using basis functions. Hum. Brain Mapp. 7 (4), 254–266.

Ashburner, J., Friston, K.J., 2000. Voxel-based morphometry—the methods. Neuroimage 11 (6 Pt. 1), 805–821.

Aylward, E.H., Habbak, R., et al., 1997a. Cerebellar volume in adults with Down syndrome. Arch. Neurol. 54 (2), 209–212.

Aylward, E.H., Li, Q., et al., 1997b. Basal ganglia volume in adults with Down syndrome. Psychiatry Res. 74 (2), 73–82.

Aylward, E.H., Li, Q., et al., 1999. MRI volumes of the hippocampus and amygdala in adults with Down's syndrome with and without dementia. Am. J. Psychiatry 156 (4), 564–568.

Baron, J.C., Chetelat, G., et al., 2001. In vivo mapping of gray matter loss with voxel-based morphometry in mild Alzheimer's disease. Neuroimage 14 (2), 298–309.

Becker, L.E., Armstrong, D.L., et al., 1986. Dendritic atrophy in children with Down's syndrome. Ann. Neurol. 20 (4), 520–526.

Burger, P.C., Vogel, F.S., 1973. The development of the pathologic changes of Alzheimer's disease and senile dementia in patients with Down's syndrome. Am. J. Pathol. 73 (2), 457–476.

Chan, D., Fox, N.C., et al., 2001. Patterns of temporal lobe atrophy in semantic dementia and Alzheimer's disease. Ann. Neurol. 49 (4), 433–442.

Deb, S., Braganza, J., 1999. Comparison of rating scales for the diagnosis of dementia in adults with Down's syndrome. J. Intellect. Disabil. Res. 43 (Pt. 5), 400–407.

Emerson, J.F., Kesslak, J.P., et al., 1995. Magnetic resonance imaging of the aging brain in Down syndrome. Prog. Clin. Biol. Res. 393, 123–138.

Evenhuis, H.M., 1996. Further evaluation of the Dementia Questionnaire for Persons with Mental Retardation (DMR). J. Intellect. Disabil. Res. 40 (Pt. 4), 369–373.

Friston, K.J., Holmes, A.P., et al., 1995. Statistical parametric maps in functional imaging: a general linear approach. Hum. Brain Mapp. 2, 189–210.

Good, C.D., Johnsrude, I.S., et al., 2001. A voxel-based morphometric study of ageing in 465 normal adult human brains. Neuroimage 14 (1 Pt. 1), 21–36.

Good, C.D., Scahill, R.I., et al., 2002. Automatic differentiation of anatomical patterns in the human brain: validation with studies of degenerative dementias. Neuroimage 17 (1), 29–46.

Haier, R.J., Chueh, D., et al., 1995. Brain size and cerebral glucose metabolic rate in non-specific mental retardation and Down Syndrome. Intelligence 20, 191–210.

Hasboun, D., Chantome, M., et al., 1996. MR determination of hippocampal volume: comparison of three methods. Am. J. Neuroradiol. 17 (6), 1091–1098.

Huxley, A., Prasher, V.P., et al., 2000. The dementia scale for Down's syndrome. J. Intellect. Disabil. Res. 44 (Pt. 6), 697–698.

Ikeda, M., Arai, Y., 2002. Longitudinal changes in brain CT scans and development of dementia in Down's syndrome. Eur. Neurol. 47 (4), 205–208.

Kang, J., Lernaire, H.G., et al., 1987. The precursor of Alzheimer's disease amyloid A4 protein resembles a cell-surface receptor. Nature 325 (6106), 733–736.

Keller, S.S., Mackay, C.E., et al., 2002. Voxel-based morphometric comparison of hippocampal and extrahippocampal abnormalities in patients with left and right hippocampal atrophy. Neuroimage 16 (1), 23–31.

Kemper, T.L., 1991. Down syndrome, in: Peters, A., Jones, E. (Eds.), Cerebral Cortex: Normal and Altered States of Function, Vol 9. Plenum, New York, pp. 511–526.

Kesslak, J.P., Nagata, S.F., et al., 1994. Magnetic resonance imaging analysis of age-related changes in the brains of individuals with Down's syndrome. Neurology 44 (6), 1039–1045.

Krasuski, J.S., Alexander, G.E., et al., 2002. Relation of medial temporal lobe volumes to age and memory function in nondemented adults with Down's syndrome: implications for the prodromal phase of Alzheimer's disease. Am. J. Psychiatry 159 (1), 74–81.

Kubicki, M., Shenton, M.E., et al., 2002. Voxel-based morphometric analysis of gray matter in first episode schizophrenia. Neuroimage 17 (4), 1711–1719.

Maguire, E.A., Gadian, D.G., et al., 2000. Navigation-related structural change in the hippocampi of taxi drivers. Proc. Natl. Acad. Sci. USA 97 (8), 4398–4403.

May, A., Ashburner, J., et al., 1999. Correlation between structural and functional changes in brain in an idiopathic headache syndrome. Nature Med. 5 (7), 836–838.

Nadel, L., 1999. Down syndrome in cognitive neuroscience perspective, in: Tager-Flusberg, H. (Ed.), Neurodevelopmental Disorders. MIT Press, Cambridge, pp. 197–222.

Pearlson, G.D., Breiter, S.N., et al., 1998. MRI brain changes in subjects with Down syndrome with and without dementia. Dev. Med. Child Neurol. 40 (5), 326–334.

Pearlson, G.D., Warren, A.C., et al., 1990. Brain atrophy in 18 patients with Down syndrome: a CT study. Am. J. Neuroradiol. 11 (4), 811–816.

Pinter, J.D., Brown, W.E., et al., 2001a. Amygdala and hippocampal volumes in children with Down syndrome: a high-resolution MRI study. Neurology 56 (7), 972–974.

Pinter, J.D., Eliez, S., et al., 2001b. Neuroanatomy of Down's syndrome: a high-resolution MRI study. Am. J. Psychiatry 158 (10), 1659–1665.

Pruessner, J.C., Li, L.M., et al., 2000. Volumetry of hippocampus and amygdala with high-resolution MRI and three-dimensional analysis software: minimizing the discrepancies between laboratories. Cereb. Cortex 10 (4), 433–442.

Raz, N., Torres, I.J., et al., 1995. Selective neuroanatomic abnormalities in Down's syndrome and their cognitive correlates: evidence from MRI morphometry. Neurology 45 (2), 356–366.

Richardson, M.P., Friston, K.J., et al., 1997. Cortical grey matter and benzodiazepine receptors in malformations of cortical development. A voxel-based comparison of structural and functional imaging data. Brain 120 (Pt. 11), 1961–1973.

Salmond, C.H., Ashburner, J., et al., 2002. Distributional assumptions in voxel-based morphometry. Neuroimage 17 (2), 1027–1030.

Schapiro, M.B., Luxenberg, J.S., et al., 1989. Serial quantitative CT analysis of brain morphometrics in adult Down's syndrome at different ages. Neurology 39 (10), 1349–1353.

Takashima, S., Ieshima, A., et al., 1989. Dendrites, dementia and the Down syndrome. Brain Dev. 11 (2), 131–133.

Talairach, J., Tournoux, P., 1988. Co-planar Stereotaxic Atlas of the Human Brain, A 3-Dimensional Proportional System: An Approach to Cerebral Imaging. Thieme, New York.

Tanzi, R.E., McClatchey, A.I., et al., 1988. Protease inhibitor domain encoded by an amyloid protein precursor mRNA associated with Alzheimer's disease. Nature 331 (6156), 528–530.

Tisserand, D., Pruessner, J., et al., 2002. Regional frontal cortical volumes decrease differentially in aging: an MRI study to compare volumetric approaches and voxel-based morphometry. Neuroimage 17 (2), 657.

Weis, S., Weber, G., et al., 1991. Down syndrome: MR quantification of brain structures and comparison with normal control subjects. Am. J. Neuroradiol. 12 (6), 1207–1211.

Wisniewski, K.E., 1990. Down syndrome children often have brain with maturation delay, retardation of growth, and cortical dysgenesis. Am. J. Med. Genet. Suppl. 7, 274–281.

Wisniewski, K.E., Dalton, A.J., et al., 1985. Alzheimer's disease in Down's syndrome: clinicopathologic studies. Neurology 35 (7), 957–961.

Worsley, K.J., Poline, J.B., et al., 1995. Tests for distributed, nonfocal brain activations. Neuroimage 2 (3), 183–194.

Wright, I.C., McGuire, P.K., et al., 1995. A voxel-based method for the statistical analysis of gray and white matter density applied to schizophrenia. Neuroimage 2 (4), 244–252.

Zellweger, H., 1977. Down syndrome, in: Vinken, P.J., Bruyn, G.W. (Eds.), Handbook of Clinical Neurology. Elsevier, New York, pp. 367–469.